LETTER

doi:10.1038/nature10779

Wetting of flexible fibre arrays

C. Duprat[1], S. Protière[2,3], A. Y. Beebe[1] & H. A. Stone[1]

Fibrous media are functional and versatile materials, as demonstrated by their ubiquity both in natural systems such as feathers[1–4] and adhesive pads[5] and in engineered systems from nanotextured surfaces[6] to textile products[7], where they offer benefits in filtration, insulation, wetting and colouring. The elasticity and high aspect ratios of the fibres allow deformation under capillary forces, which cause mechanical damage[8], matting[5,9] self-assembly[10,11] or colour changes[12], with many industrial and ecological consequences. Attempts to understand these systems have mostly focused on the wetting of rigid fibres[13–17] or on elastocapillary effects in planar geometries[18] and on a fibre brush withdrawn from an infinite bath[19]. Here we consider the frequently encountered case of a liquid drop deposited on a flexible fibre array and show that flexibility, fibre geometry and drop volume are the crucial parameters that are necessary to understand the various observations referred to above. We identify the conditions required for a drop to remain compact with minimal spreading or to cause a pair of elastic fibres to coalesce. We find that there is a critical volume of liquid, and, hence, a critical drop size, above which this coalescence does not occur. We also identify a drop size that maximizes liquid capture. For both wetting and deformation of the substrates, we present rules that are deduced from the geometric and material properties of the fibres and the volume of the drop. These ideas are applicable to a wide range of fibrous materials, as we illustrate with examples for feathers, beetle tarsi, sprays and microfabricated systems.

Owing to the numerous environmental and industrial applications of fibrous media, their wetting has been studied extensively. Most research focuses on drops or flow on individual rigid fibres, often in an array. However, in most applications, the elasticity of the fibres is important, as evidenced from the matting of feather barbules[9], the shrinkage of porous fibre membranes[8], strengthening of paper after drying[20], the clumping of the setae of beetle tarsi after release of tarsal oil[5], or the collapse of micro- or nanopillar arrays[10–12]. Therefore, we are motivated by the interaction of a mist of drops with a deformable, or flexible, array of fibres. The basic elastocapillary response is observed in the behaviour of a liquid drop on a pair of fibres, which is where we begin.

For a perfectly wetting drop (that is, a drop that connects with the fibre with a zero contact angle) deposited on two parallel, rigid fibres, the minimization of surface energy yields three distinct drop shapes depending on the ratio of the distance between the fibres, $2d_0$ (measured from their outer surfaces), and their diameter, $2r$ (Fig. 1b). As d_0/r is decreased, the drop evolves from a bridge to a barrel shape and then spreads out into a liquid column[13–17]: a drop forms for $d_0/r > \sqrt{2}$, a column forms for $d_0/r < 0.57$ and there is non-uniqueness of the shape for $0.57 < d_0/r < \sqrt{2}$.

In this Letter, we investigate the behaviour of a perfectly wetting drop deposited onto two horizontal, flexible fibres that at one end are clamped, parallel to each other, a distance $2d_0 > 2\sqrt{2}r$ apart and at the other end are free to move (Methods and Fig. 1a). Our results can be extended to the case of partial wetting by adding as an additional parameter the effective contact angle, $\theta < \pi/2$ (Supplementary Fig. 4). We neglect gravitational effects because the fibres do not bend under their own weight and the drop sizes are smaller than the capillary length, l_c, above which gravitational effects become important. By $2d$ we denote the distance between the fibres at the drop location. When the drop is placed on the fibres close to the clamped ends, the fibres deflect inwards and the drop moves spontaneously towards the free ends, which are closer together (Fig. 1c and Supplementary Movie 2), as observed for a drop in a wedge[21]. As the drop advances, the deflection increases, that is, d/r continuously decreases. The drop accelerates, elongates and then spreads spontaneously between the fibres, drawing them together finally to form a liquid column between coalesced fibres.

We performed a large set of experiments to characterize the final state as a function of the drop volume, V; the fibre length, L; and the ratio d_0/r (Methods). For every value of d_0/r, we find three different final states as L and V are varied (Fig. 2a–c). Whereas the final state (drop or column) of a finite volume of liquid deposited on two rigid fibres depends on only one parameter, that is, d_0/r, and is hence independent of the drop volume and fibre length, we find that the final equilibrium state for a drop on two flexible fibres depends on six

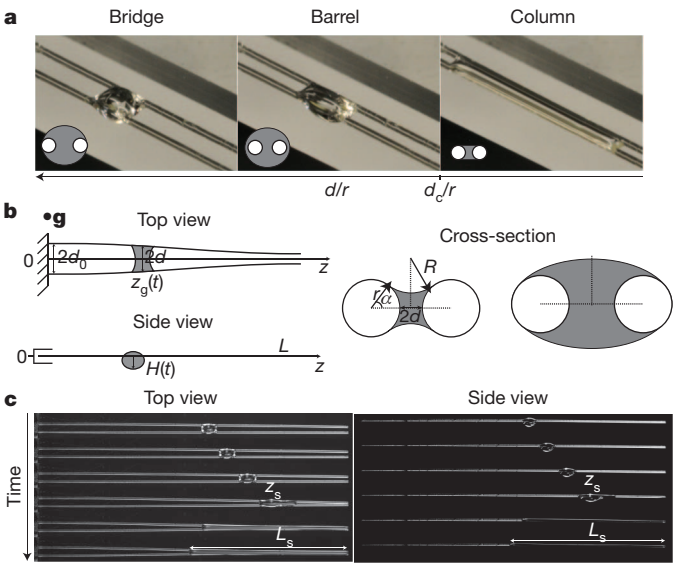

Figure 1 | Shape transitions of a drop sitting on two parallel fibres. a. A drop of perfectly wetting liquid (silicone oil) of volume 2 μl deposited on two parallel, rigid glass fibres (radius, $r = 0.145$ mm) adopts three different shapes depending on the distance between the fibres: a 'bridge' ($d_0/r = 2.5$), a 'barrel' ($d_0/r = 1.5$) and a column ($d_0/r = 1$). d_c, critical distance at which the drop-to-column transition occurs. **b**, Experimental set-up used to investigate the behaviour of a drop deposited on two flexible fibres, which are clamped at one end and free to move at the other. Left: top and side views, recorded simultaneously using a mirror. Right: expected cross-sections for a concave liquid column and a convex drop. The direction of gravity is indicated by **g**. **c**, Typical experiment with $d_0/r = 2.7$, $V = 1.5$ μl and $L = 4$ cm. The time between successive images is 25 s. When the drop is deposited on flexible fibres, the fibres deflect inward. The drop spontaneously moves towards the free ends of the fibres. At a given location, z_s, the drop starts spreading and the fibres are drawn together. The final wet length is denoted L_s.

[1]Department of Mechanical and Aerospace Engineering, Princeton University, Princeton, New Jersey 08544, USA. [2]CNRS, UMR 7190, Institut Jean le Rond d'Alembert, F-75005 Paris, France. [3]UPMC Université Paris 06, UMR 7190, Institut Jean le Rond d'Alembert, F-75005 Paris, France.

©2012 Macmillan Publishers Limited. All rights reserved

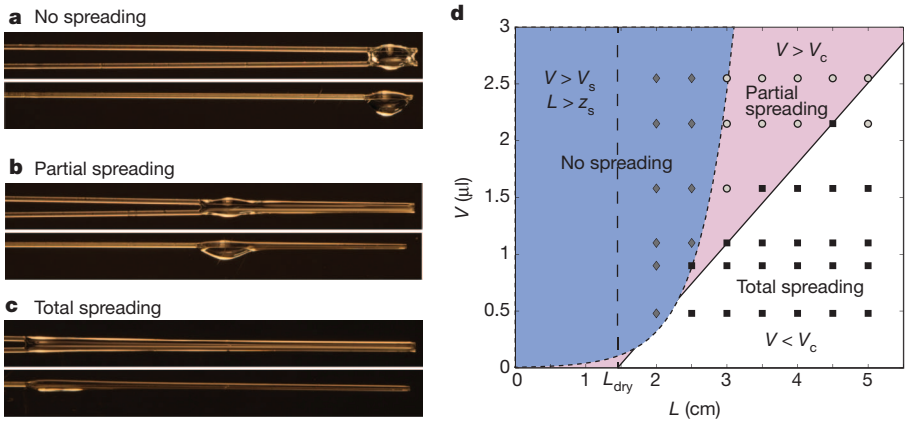

Figure 2 | The three different final states of a drop between two flexible fibres. **a**–**c**, Top and side views of the final state obtained for $d_0/r = 2.6$; a fixed volume, $V = 2$ µl; and increasing length, $L = 3$, 3.5 and 4 cm. The final state changes from one of no spreading to one of partial spreading to one of total spreading as L increases. **d**, Phase diagram of the different regimes for $d_0/r = 2.1$. Depending on L and V, three different regimes are observed: the drop either moves towards the ends without spreading (diamonds; **a**), spreads until partial depletion of the drop (circles; **b**) or spreads completely into a liquid column (squares; **c**). The solid and dashed curves correspond to equations (2) and (3), respectively. The vertical dashed line corresponds to $L = L_{dry}$.

parameters: r; d_0; L; the bending stiffness, B, of the fibre; the surface tension, γ; and V. For short fibres ($L \ll 2$ cm in the system presented in Fig. 2) and almost all drop volumes, the fibres deflect slightly inwards and the drop moves towards the free ends, but there is no spreading (Fig. 2a and Supplementary Movie 1). For longer fibres, there is a range of drop volumes such that when we increase L, the deflection increases and the whole drop spreads into a column ('total spreading'; Fig. 2c and Supplementary Movie 2). Alternatively, for sufficiently large volumes, we observe a state of 'partial spreading', where there is a liquid column with a smaller drop remaining at the edge (Fig. 2b and Supplementary Movie 3). We summarize in Fig. 2d our results in a phase diagram of V versus L, which suggests that a critical size of drops in a spray can trigger coalescence of a fibrous material.

To understand the transitions between the different regimes in Fig. 2d, we first consider the case of long fibres, for which either partial or total spreading occurs for all volumes investigated. We fix the fibre length and measure the length, L_s, along which the liquid spreads for various drop volumes (Fig. 3a). For small V, the whole drop spreads into a liquid column. As V increases, the column length increases until, above a critical volume, V_c, a drop remains at the wider end of the column and the length L_s actually decreases (Fig. 3a). The existence of a maximum spreading length here is a consequence of elasticity.

We can understand the maximum spreading length, $L_{s,max}$, reached at V_c as a balance between elasticity and capillarity. There is a minimal distance, L_{dry}, along which the dry portions of the fibres can be bent by capillary forces. This is determined by minimizing the total energy of the system[22], yielding

$$L_{dry} = \left(\frac{9Bd_0^2}{2\gamma r S(\alpha)}\right)^{1/4} \quad (1)$$

where $S(\alpha)$ is a geometric factor evaluated approximately for a flat liquid column as $S(\alpha = \pi/2) = \pi - 2$. This length is the minimum length of the fibres beyond which collapse, or significant deformation, can occur. For a given d_0/r ratio, L_{dry} is constant and the maximum wet length, $L_{s,max}$, increases linearly with L, that is, $L_{s,max} = L - L_{dry}$, in agreement with our experiments (Supplementary Fig. 1). This elastocapillary balance results in an optimal, or critical, drop volume for which the spreading length is maximal: $V_c = A(\alpha)L_{s,max}$, where $A(\alpha)$ is the column cross-section ($A(\pi/2) \approx \pi r^2$ for a flat column). The boundary between total and partial spreading is then predicted to be

$$V = V_c = \pi r^2 (L - L_{dry}) \quad (2)$$

which is also in agreement with the experimental transition (Fig. 2d). When liquid is added to this maximum column (Supplementary Fig. 2), the configuration is unstable: the liquid forms a drop at the wider end of the column. Minimization of the surface energy causes the liquid to retract to form this spherical drop, decreasing the length of the column.

To understand the critical drop size beyond which no spreading (Fig. 2a) and, hence, no fibre coalescence occurs, we measured the spacing, d_s, at which the drop starts spreading. We find that the ratio

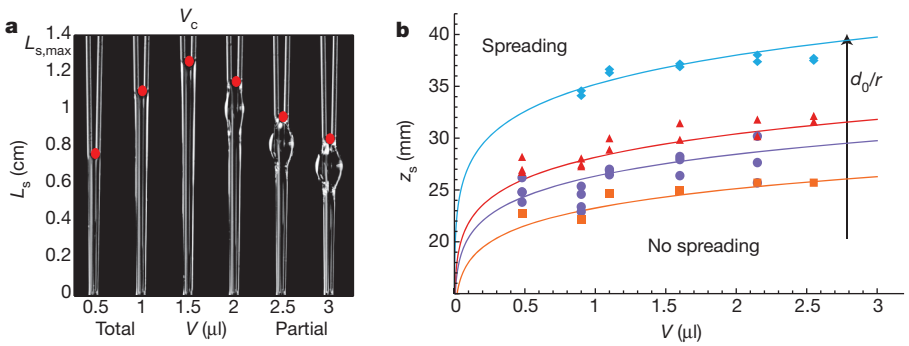

Figure 3 | Influence of the initial drop volume on the final state. **a**, Transition between total and partial spreading: evolution of the spreading length, L_s, with the volume, V, of the drop for $d_0/r = 2.6$ and $L = 3.5$ cm. We observe an optimum (maximum L_s) at a critical volume of $V_c = 1.5$ µl. **b**, Transition between spreading and no spreading: evolution of the position of the drop at spreading, z_s, with V for $d_0/r = 1.9$ (orange), 2.4 (purple), 2.7 (red) and 4.2 (blue). The position of the drop at spreading is independent of the fibre length and increases with increasing volume, spacing and fibre rigidity (that is, the bending modulus, which is proportional to r^4). The solid lines correspond to the theoretical prediction (Supplementary Information, equation (2)).

©2012 Macmillan Publishers Limited. All rights reserved

$d_s/r = 1.11 \pm 0.07$ is constant, independent of V, L and d_0/r. We conclude that spreading occurs when locally the spacing between the fibres is such that a liquid column is energetically favourable relative to a drop. This criterion for spreading is similar to that obtained theoretically for rigid fibres[13] and similar to that found in our experiments on rigid glass fibres: $d_s/r = 1.04 \pm 0.07$.

Next we estimated the critical drop volume responsible for this spreading, where liquid is captured in a column. The drop is in a barrel shape (Fig. 1a) and thus is pierced by the two fibres. The capillary force applied by the drop, $F \approx 2\gamma l^*$, where l^* is the typical length of the contact line, brings the fibres together. Coalescence of fibres will therefore occur if F is great enough to achieve a deflection of $d_0 - d_s$ along the fibres, that is, if the capillary torque, Fz_s, where z_s is the position of the drop, equals the elastic resisting torque, $B(d_0 - d_s)/z_s^2$. For a given value of V and, hence, F, this estimate leads to a critical drop position, $z_s^3 \propto B(d_0 - d_s)/F$, below which no spreading will occur, which is also verified experimentally (Fig. 3b). For a fixed value of d_0, z_s increases with increasing volume and, hence, the capillary force decreases. Therefore, for a given fibre length, there is a minimal force, that is, a maximal drop volume, for spreading to occur, set by $z_s = L$. The force $F \approx 2\gamma l^*$ depends on the complex shape of the contact line, which has a typical length $l^* \propto 2\pi r d_s V^{-1/3}$ (Supplementary Information). Combining these results yields the critical volume for spreading

$$V_s \approx \left(\beta \frac{\gamma d_s r L^3}{B(d_0 - d_s)}\right)^3 \qquad (3)$$

where the constant β depends only on the complex shape of the drop (Supplementary Fig. 3); this result involves all of the geometric and material properties. The boundary between the regimes of spreading and no spreading, $V = V_s$, is in agreement with the experiments (Fig. 2d).

Because the final state of the drop placed on the fibre array depends on the six parameters r, d_0, L, B, γ and V, we conclude by dimensional analysis that the system is characterized by three parameters, $L/L_{s,max}$, V/V_c and d_0/r where $L_{s,max} = L - L_{dry}$ (from equation (1)) and $V_c = \pi r^2 L_{s,max}$ (from equation (2)). We define a phase diagram of the three possible final states in the space of the two parameters $L/L_{s,max}$ and V/V_c (Fig. 4a). First we identify a threshold, $V/V_c = 1$, below which a drop will always totally spread, which maximizes the wetted length and the amount of trapped liquid. Second, for $V/V_c > 1$, the spreading is partial: the remaining edge drop can be shed by any perturbation such as shaking, which results in a smaller amount of liquid being captured by the fibre array. The transition from spreading to no spreading ($V > V_s$) is identified by equation (3) and depends on the parameter d_0/r as reflected by the successive hyperbolic curves in Fig. 4a. For partial wetting, θ, the effective contact angle, should be included in equations (1), (2) and (3) (Supplementary Information and Supplementary Figs 4–7). All of the experimental data (symbols in Fig. 4a) obtained by varying all of the parameters are well within each regime defined by the model.

This map allows us to predict the interaction of natural or engineered fibrous materials with a mist of drops. An example of a natural fibre array is a bird feather, which consists of well-ordered hair-like structures (barbs and barbules) that produce hydrophobicity and thermal insulation[1,3]. Small amounts of oil disrupt this arrangement by clumping adjacent barbules, affecting their water repellency and insulating properties and thus reducing the survival rate of oiled birds[9,23]. We sprayed a polydisperse aerosol of oil on goose feathers and observed all three possible final states (Fig. 4b). Using our model system, we find that a volume of oil less than V_c (here a drop radius less than 20 μm) spreads, thus clumping adjacent barbules and making the cleaning process difficult. Drops larger than V_s (drop radius, 140 μm) do not spread and may be dislodged from the bird's plumage. These results are in agreement with our map (Fig. 4a). Despite complex initial conditions (multiple fibres and/or drops, different wettabilities or surface roughnesses) the final states can thus be captured by our model and we can predict the main effects arising when a mist of drops interacts with a dilute fibre array.

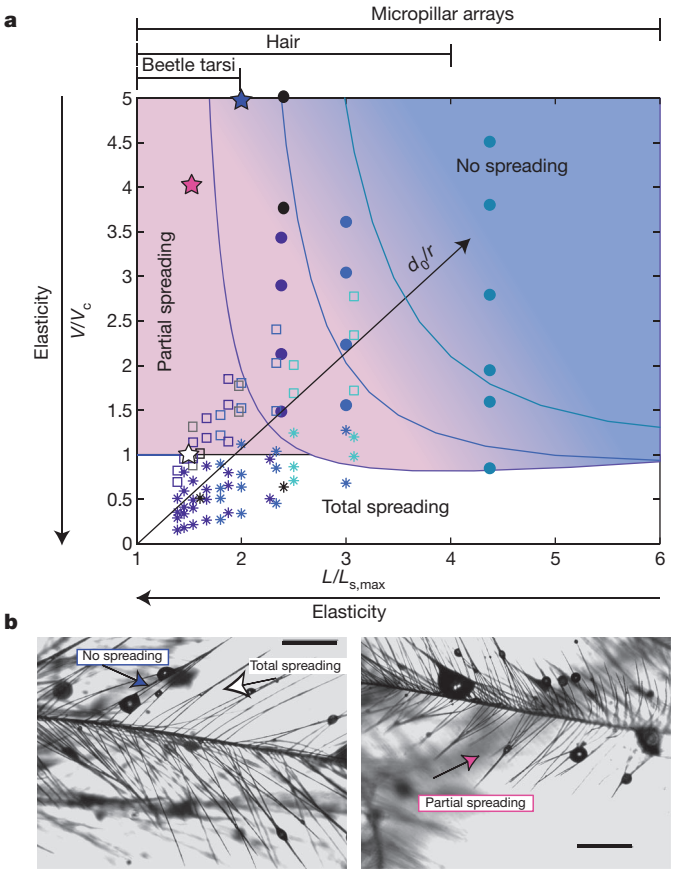

Figure 4 | Aerosol size and fibre matrix properties needed to collect, trap or displace a known volume of liquid. a, Map of the three spreading regimes as a function of the two dimensionless parameters $L/L_{s,max}$ and V/V_c. The solid curves show three limits for $d_0/r = 2.4$, 2.7 and 4.2 and the points show data for total spreading (asterisks), partial spreading (squares) and no spreading (circles) of silicone oil (total wetting, $d_0/r = 2.1$; blue and purple points) and water (partial wetting, $d_0/r = 3$; black and grey points). Stars correspond to the three situations observed in **b**. **b**, Microscope pictures of goose feathers sprayed with oil (smaller drops have volumes of order 10^{-14}–10^{-13} m^3), showing no spreading ($d_0/r = 4.8$, $L/L_{s,max} = 2$, $V/V_c \approx 5$; blue star in **a**), total spreading ($d_0/r = 3.4$, $L/L_{s,max} = 1.5$ and $L_s = L_{s,max} = 0.8$ mm; white star in **a**) and partial spreading ($d_0/r = 3.5$, $L/L_{s,max} = 1.5$, $V/V_c \approx 4$; pink star in **a**) in agreement with our predictions. Scale bars, 500 μm.

In addition, aerosol-removal filters, hairsprays, adhesive pads for insects and some applications in microstructure design require total spreading, that is, optimal coating of the fibres or maximal liquid capture. Conversely, fibres in living systems may have evolved a certain length or material properties to adapt to their environmental conditions. For example, we can now use our model to make quantitative estimates for various fibrous media and liquids (Supplementary Table 1) as reported in the universal map (Fig. 4a). For beetles, we predict that drops of optimal diameter 5 μm released from ventral pores travel along the setae and spread totally (that is, without liquid loss) where the tarsi contact a substrate; we predict that the collapse of pillars in microfabrication, observed during solvent evaporation[10–12], could be controlled by depositing an optimum volume of liquid (drops of diameter 0.9–5.4 μm); and we predict that microstructures could be designed to respond (by changing colour) to aerosols of different drop sizes because light scattering is influenced by clustering of the microelements. These examples illustrate the wide range of flexible systems that could be controlled using elastocapillarity and an optimally chosen drop volume.

©2012 Macmillan Publishers Limited. All rights reserved

METHODS SUMMARY

The glass fibres (radius, $r = 0.145$ mm; bending stiffnesses, $B = 1 \times 10^{-6}$ N m^2 and $B = 7 \times 10^{-7}$ N m^2; length, 2 cm $< L <$ 5.5 cm) are clamped at one end, separated by a distance $2d_0$ ($d_0/r = 1.9, 2.1, 2.6$ and 4.3). A drop of silicone oil (viscosity, $\eta = 97$ mPa s; density, $\rho = 970$ kg m^{-3}; surface tension, $\gamma = 0.021$ N m^{-1}) of controlled volume V (0.48 µl $< V <$ 2.55 µl) precise to 5% for large volumes and to 10% for smaller volumes, is deposited onto the fibres with a micropipette, close to the clamped edge. The positions of the front, $z_f(t)$, and the rear, $z_r(t)$, of the drop (relative to the clamped end at $z = 0$), as well as the distance between the fibres, d, are recorded from the top with a digital camera. A mirror placed at 45° allows us to capture a simultaneous side view of the drop and measure its size, $H(z, t)$. We define the average position of the drop as $z_g = (z_f + z_r)/2$, and its length is $l = z_f - z_r$. The capillary length, $l_c = (\gamma/\rho g)^{1/2}$, is the length beyond which gravitational effects become more important than capillary effects. Here $l_c = 1.5$ mm.

Received 8 August; accepted 6 December 2011.

1. Rijke, A. M. & Jesser, W. A. The feather structure of dippers: water repellency and resistance to water penetration. *Wilson J. Ornithol.* **122,** 563–568 (2010).
2. Rijke, B. Y. A. M. The water repellency and feather structure of cormorants, Phalacrocoracidae. *J. Exp. Biol.* **48,** 185–189 (1968).
3. Dawson, C., Vincent, J., Jeronimidis, G., Rice, G. & Forshaw, P. Heat transfer through penguin feathers. *J. Theor. Biol.* **199,** 291–295 (1999).
4. Zi, J. *et al.* Coloration strategies in peacock feathers. *Proc. Natl Acad. Sci. USA* **100,** 12576–12578 (2003).
5. Eisner, T. & Aneshansley, D. J. Defense by foot adhesion in a beetle (Hemisphaerota cyanea). *Proc. Natl Acad. Sci. USA* **97,** 6568–6573 (2000).
6. Liu, K. & Jiang, L. Bio-inspired design of multiscale structures for function integration. *Nano Today* **6,** 155–175 (2011).
7. Eadie, L. & Ghosh, T. K. Biomimicry in textiles: past, present and potential. An overview. *J. R. Soc. Interface* **6,** 761–775 (2011).
8. Kamo, J., Hiram, T. & Kamada, K. Solvent-induced morphological change of microporous hollow fiber membranes. *J. Membr. Sci.* **70,** 217–224 (1992).
9. O'Hara, P. D. & Morandin, L. A. Effects of sheens associated with offshore oil and gas development on the feather microstructure of pelagic seabirds. *Mar. Pollut. Bull.* **60,** 672–678 (2010).
10. Pokroy, B., Kang, S. H., Mahadevan, L. & Aizenberg, J. Self-organization of a mesoscale bristle into ordered, hierarchical helical assemblies. *Science* **323,** 237–240 (2009).
11. Chandra, D. & Yang, S. Stability of high-aspect-ratio micropillar arrays against adhesive and capillary forces. *Acc. Chem. Res.* **43,** 1080–1091 (2010).
12. Chandra, D., Yang, S., Soshinsky, A., a. & Gambogi, R. J. Biomimetic ultrathin whitening by capillary-force-induced random clustering of hydrogel micropillar arrays. *ACS Appl. Mater. Interfaces* **1,** 1698–1704 (2009).
13. Princen, H. Capillary phenomena in assemblies of parallel cylinders III. Liquid columns between horizontal parallel cylinders. *J. Colloid Interface Sci.* **34,** 171–184 (1970).
14. Wu, X.-F., Bedarkar, A. & Vaynberg, K. A. Droplets wetting on filament rails: surface energy and morphology transition. *J. Colloid Interface Sci.* **341,** 326–332 (2010).
15. Bedarkar, A., Wu, X.-f. & Vaynberg, A. Wetting of liquid droplets on two parallel filaments. *Appl. Surf. Sci.* **256,** 7260–7264 (2010).
16. Minor, F. W., Schwartz, M., Wulkow, E., a. & Buckles, L. C. Part III: The behavior of liquids on single textile fibers. *Text. Res. J.* **29,** 940–949 (1959).
17. Keis, K., Kornev, K. G., Kamath, Y. K. & Neimark, A. V. in *Nanoengineered Nanofibrous Materials* (eds Guceri, S., Gogotsi, Y. G & Kuznetsov, V.) 173–180 (Kluwer, 2004).
18. Kwon, H.-M., Kim, H.-Y., Puëll, J. R. M. & Mahadevan, L. Equilibrium of an elastically confined liquid drop. *J. Appl. Phys.* **103,** 093519 (2008).
19. Roman, B. & Bico, J. Elasto-capillarity: deforming an elastic structure with a liquid droplet. *J. Phys. Condens. Matter* **22,** 493101 (2010).
20. Hubbe, M. A. Bonding between cellulosic fibers in the absence and presence of dry-strength agents - a review. *BioResources* **1,** 281–318 (2006).
21. Prakash, M., Quéré, D. & Bush, J. W. M. Surface tension transport of prey by feeding shorebirds: the capillary ratchet. *Science* **320,** 931–934 (2008).
22. Py, C., Bastien, R., Bico, J., Roman, B. & Boudaoud, A. 3D aggregation of wet fibers. *Europhys. Lett.* **77,** 44005 (2007).
23. Hartung, R. Energy metabolism in oil-covered ducks. *J. Wildl. Mgmt* **31,** 798–804 (1967).

Supplementary Information is linked to the online version of the paper at www.nature.com/nature.

Acknowledgements C.D. and H.A.S. acknowledge Unilever and the NFS for financial support. S.P. acknowledges financial support from the Emergence(s) Program of the City of Paris and CNRS and thanks Princeton University for its hospitality. We thank A. Lips and P. Warren for comments.

Author Contributions C.D. and S.P. designed the experiments; A.Y.B., C.D. and S.P. carried out the experiments; C.D., S.P. and H.A.S. discussed and interpreted the results; C.D. and H.A.S. developed the models; and C.D., S.P. and H.A.S. wrote the manuscript.

Author Information Reprints and permissions information is available at www.nature.com/reprints. The authors declare no competing financial interests. Readers are welcome to comment on the online version of this article at www.nature.com/nature. Correspondence and requests for materials should be addressed to H.A.S. (hastone@princeton.edu).

©2012 Macmillan Publishers Limited. All rights reserved